Rare Metal Materials and Engineering
Volume 55, Issue 7, July 2026
Available online at www.rmme.ac.cn

Science Press

Cite this article as: Feng Jun, Deng Shengyong, Zhao Yingchao, et al. Preparation and Properties of Nano-hydroxyapatite-Doped Micro/nano-structured Micro-arc Oxidized Composite Coating for Pure Titanium[J]. Rare Metal Materials and Engineering, 2026, 55(07): 1651-1663. DOI: https://doi.org/10.12442/j.issn.1002-185X.20250404.

ARTICLE

Preparation and Properties of Nano-hydroxyapatite-Doped Micro/nano-structured Micro-arc Oxidized Composite Coating for Pure Titanium

Feng Jun, Deng Shengyong, Zhao Yingchao, Cheng Junjie, Yang Xudong

College of Mechanical Engineering, University of South China, Hengyang 421001, China

Abstract: Micro/nano-structured composite coating composed of titanium dioxide (TiO_2) and hydroxyapatite (HA) was fabricated on TA2 pure titanium through synergistic micro-arc oxidation (MAO) and hydrothermal (HT) processing to enhance the corrosion resistance and biocompatibility of titanium substrates. The surface micromorphology of the coatings was investigated by scanning electron microscope; the roughness and hydrophilicity of the coatings were investigated by atomic force microscope and water contact angle, respectively; the corrosion resistance was evaluated by electrochemical impedance spectroscopy and potentiodynamic polarization tests in simulated human body fluids; the biocompatibility was investigated by in-vitro cell culture experiments. Results demonstrate that by doping HA into MAO electrolyte, a micrometer-sized coating loaded with nano-HA particles can be obtained, and then HT treatment can be conducted to obtain the micro/nano-structured composite coating with a HA-containing nanoflake structure. This micro/nano-structured composite coating possesses good hydrophilicity and fine corrosion resistance. The coating performance achieves optimal state when the coating is prepared with 3 g/L HA and HT-treated for 6 h. In this case, the water contact angle is as low as 24.2°, and the polarization resistance is as high as 2.467×10^4 Ω·cm^2. In addition, the synergistic effect of nano-HA and micro/nano-structure on the coating surface greatly promotes the cell proliferation, presenting non-cytotoxic characteristic, and indicating that the coating possesses good biocompatibility.

Key words: micro-arc oxidation; HT method; nano-HA; micro/nano-structure

1 Introduction

Titanium and its alloys have emerged as a new generation of biomedical implant materials due to their excellent mechanical properties, non-magnetic nature, and non-toxicity[1–4]. Pure titanium possesses the density and elastic modulus comparable to those of human bone. This similarity can assist in mitigating the stress concentration generated by the implant during in-vivo activities, thereby reducing the risk of bone loss and necrosis due to the stress shielding effect. However, titanium demonstrates suboptimal biocompatibility and corrosion resistance in physiological environment. Titanium is susceptible to body fluids, and the implant materials may move in human body[5–7]. The fabrication of functional coatings on pure titanium surfaces can enhance their comprehensive properties. Titanium and its alloys have been extensively investigated as promising candidates for implant materials due to their favorable mechanical properties and biocompatibility. However, the insufficient bioactivity, poor corrosion resistance, and inadequate wear resistance of titanium and titanium alloy implant materials need to be solved in clinical applications.

To achieve enhanced medical efficacy, the performance requirements for biomaterials have become increasingly stringent. The smooth and non-porous surface of untreated pure titanium results in its insufficient cell adhesion capacity. To solve this problem, researchers have used various surface modification techniques to adjust the surface properties and chemical structure of titanium implants to improve the corrosion resistance and biocompatibility, including plasma

Received date: July 31, 2025
Foundation item: National Natural Science Foundation of China (52305313)
Corresponding author: Feng Jun, Ph. D., Associate Professor, College of Mechanical Engineering, University of South China, Hengyang 421001, P. R. China, E-mail: speedfjkang@163.com

spraying[8–9], micro-arc oxidation (MAO) [10–11], ion implantation[12], and magnetron sputtering technique[13–14]. Among them, MAO is regarded as a promising technique for surface treatment. This method can produce ceramic coatings on metal surfaces that are micron-sized, porous, rough, and hard, including titanium, aluminum, magnesium, tantalum, and their alloys[15]. Selvi et al[16] prepared a MAO coating with higher seismic performance on the surface of AZ91 alloy by optimizing electrolyte composition and electrical parameters. It is reported that compared with the AZ91 alloy substrate, the equivalent thermal conductivity of the coating can be reduced by 30%. Zhu et al[17] used MAO technique to prepare a relatively dense coating on the surface of AZ91D magnesium alloy, and they found that the denser the MAO ceramic coating on magnesium alloy, the better the corrosion resistance.

It has been commonly recognized that the nano-structure surfaces can improve protein adsorption, consequently modifying cellular behavior and facilitating the adhesion, proliferation, and differentiation of osteogenic cells[18–19]. Although there are many methods for fabricating micro/nano-structured coating on titanium-based metal surfaces, the problems of weak bonding strength, equipment complexity, high cost, and prolonged growth cycles still remain unresolved. Therefore, selecting a simple and efficient approach to construct micro/nano-structure on material surfaces to enhance the biocompatibility has become critically important. Hydrothermal (HT) treatments are widely used because they are simple, efficient, and environmentally friendly, and they can adjust temperature and pressure during processing[20–21]. HT method facilitates the formation of a diverse range of nano-structures, such as nano-protuberances/particles, nano-rods, and nano-tubes, and it also allows the doping of various bioactive elements on the surface for the preparation of multifunctional biomaterials. It is demonstrated that the nanoscale (<1 μm) particles of coating on the surfaces of titanium or its alloy can significantly enhance the osteoblast adhesion[22]. Therefore, MAO-assisted HT technique has become a key research focus to construct composite coatings with micro/nano-structures and controllable chemical composition on titanium substrates in the implant field.

Hydroxyapatite (HA), a basic calcium phosphate, is one of the main components of human bones. It can form chemical bonds on biological tissues and release harmless ions into the body, therefore participating in metabolism, helping to repair damaged tissues, and demonstrating a certain level of bioactivity. It is demonstrated that HA coating can significantly reduce the corrosion rate of titanium and its alloys while exhibiting bone conduction performance[23]. Li et al[24] prepared a HA-doped coating on the surface of AZ31 magnesium alloy by MAO method. The prepared coating showed a significant enhancement in the proliferation of MC3T3-E1 cells and presented effectively improved biocompatibility. Xu et al[25] fabricated a HA/TiO composite coating on the surface of titanium alloy using MAO method and investigated the influence of Ca/P ratio in the electrolyte on coating performance. The results demonstrated that an appropriate increase in the Ca/P ratio within the electrolyte can effectively promote HA formation, thereby enhancing the corrosion resistance and biological activity of the coating.

In summary, the micro/nano-structures of titanium surface offer significant advantages in terms of biocompatibility and corrosion resistance, which can greatly promote the cell proliferation. Furthermore, the incorporation of nano-HA particles enhances the cellular activity and further improves the corrosion resistance of the coating. Currently, Li et al[26] have formed a composite coating containing HA on a titanium surface by MAO coupled with sol-gel method. However, no further nanoscale treatment has been applied to the coating, and few studies have explored the bio-coatings containing HA and possessing the micro/nano-structures. Therefore, in this research, a composite coating doped with nano-HA particles of micro/nano-structures was prepared on the pure titanium surfaces through a two-step MAO-HT process. This process enhanced the corrosion resistance of titanium and achieved good porosity of titanium, exerting the synergistic effects of the micro/nano-structured coatings, and resulting in excellent cell proliferation. This research provided guidance for the development of new implant materials.

2 Experiment

The substrate was selected from a wire-cut TA2 pure titanium metal (Guantai Metal Materials Co., Ltd, China) with dimension of 25 mm×50 mm×2.5 mm. The chemical composition of TA2 pure titanium is shown in Table 1, and Table 2 shows the chemical reagents used in this research.

TA2 pure titanium metal sample (25 mm×50 mm×2.5 mm) was selected as the substrate. The substrate was sequentially ground and polished using metallographic abrasive paper of

Table 1 Chemical composition of TA2 pure titanium (wt%)

Ti	Fe	C	N	H	O
99.29	0.30	0.10	0.05	0.015	0.25

Table 2 Chemical reagents used in this research

Chemical reagent	Chemical formula	Purity specification	Manufacturer
Absolute ethanol	C_2H_5OH	Analytically pure	Sinopharm Chemical Reagent Co., Ltd
Acetone	CH_3COCH_3	Analytically pure	Chengdu Union Chemical Industry Co., Ltd
Sodium hydroxide	NaOH	Analytically pure	Sinopharm Chemical Reagent Co., Ltd
Sodium tetraborate	$Na_2B_4O_7$	Analytically pure	Sinopharm Chemical Reagent Co., Ltd
HA	$Ca_5(PO_4)_3OH$	Analytically pure	Shanghai Yika Biological Technology Co., Ltd

200#, 600#, 800#, and 1000# until achieving an oxide-free mirror finish, followed by ultrasonic cleaning in acetone and absolute ethanol for 15 min to remove the surface oil contaminants. Then, the substrate was washed by deionized water to ensure its readiness for the natural air-drying process. MAO process used the equipment developed by the Southwest Institute of Physics of Nuclear Industry (China), including power supply, stainless steel electrolysis tank, water cooler, and compressor. The reaction process through the water cooler was used to control the electrolyte temperature ≤25 °C. The experiment was conducted in constant-current mode with the power supply parameters set at current density of 16 A/dm^2, duty cycle of 10%, and frequency of 500 Hz. MAO reaction time was maintained at 20 min for all samples. The electrolyte of 0.15 mol/L NaOH+0.1 mol/L $Na_2B_4O_7$ was selected for the doping experiment with nano-HA particles (particle size of 20–50 nm). The electrolyte was stirred before the experiment in the numerically control ultrasonic cleaning machine for 3 h, and continuous stirring was maintained during the whole MAO process. In constant current mode, the current density, duty cycle, and frequency were set to 16 A/dm^2, 10%, and 500 Hz, respectively. The reaction time of MAO was controlled at 20 min. The porous micro/nano-structured coatings prepared through the aforementioned electrolyte (0.15 mol/L NaOH+0.1 mol/L $Na_2B_4O_7$) and nano-HA (3 g/L) doping were subjected to HT treatment, separately. Through preliminary exploration, during HT process, the concentration of NaOH was 0.5 mol/L, the pH value of the solution was 12.5 – 13.8, and the reaction temperature was 170 °C. The coated sample was placed in a HT reaction container with polytetrafluoroethylene. The reaction container was heated in an oven at 170 °C for 3, 6, and 12 h. After the reaction was completed, the reaction container was naturally cooled to room temperature, and then the sample was taken out and rinsed with deionized water for natural air drying.

Scanning electron microscope (SEM, ZEISSGemini SEM300, Germany) was employed to examine the surface morphology of the coating with an acceleration voltage of 15 kV and a working distance ranging from 10 mm to 15 mm. The elemental composition was analyzed using the energy-dispersive spectrometer (EDS) attached to SEM, operating at an acceleration voltage of 20 kV. The surface roughness of the coating was observed using an atomic force microscope (AFM, Bruker Dimension Icon, Germany) with test area of 1 μm×1 μm. Image J software was used to calculate the porosity of the coating surface, and the surface of the randomly selected samples was tested 10 times to obtain the average result. The phase composition of the coating surface was analyzed using an X-ray diffraction (XRD) analyzer (Rigaku Smartlab, Japan) with the following diffraction conditions: Cu-Kα radiation, operating voltage of 40 kV, operating current of 40 mA, scanning rate of 2°/min, and 2θ= 10°–80°.

The contact angle tester (CA, Lauda Scientific LSA100, Germany) was employed to determine the water contact angle of the samples. The 2 μL-type water droplet was used. Five distinct points on the sample surface were chosen for measurement, and any outliers were excluded before calculating the average value.

The CS300M electrochemical workstation was employed to measure the dynamic potential polarization curves of the samples in Hank's solution, namely simulated human body fluid. A three-electrode system was used, where the sample served as the working electrode, the saturated calomel electrode served as the reference electrode, and the platinum electrode (10 mm×10 mm) served as the auxiliary electrode. The scan rate was set at 0.01 V/s.

Cell viability assays were performed using preosteoblasts from mouse (MC3T3-E1). The cell suspension was prepared at a density of 3×10^4 cells/cm^2. Subsequently, the cell suspension was dispensed into the sample wells, and the cultures were maintained for 1, 3, and 5 d. After the culture periods, live/dead staining was conducted, and the stained cells were observed under a fluorescence microscope (Leica DM68, Germany). Cell proliferation experiments were performed using MTT assay. Thiazolyl blue was dissolved in phosphate-buffered saline with concentration of 1 mg/mL, and it was added to each culture well. After culture at a constant temperature for 4 h, 150 μL dimethyl sulfoxide was introduced into each well and mixed by low-speed shaking for 10 min. After complete dissolution, the absorbance values were measured and statistically analyzed using an enzyme-linked immunosorbent assay instrument (DG3022A).

3 Results and Discussion

3.1 Microstructures of MAO coatings

Fig. 1 shows SEM images of the undoped and nano-HA-doped MAO coatings. Fig. 1a shows the microstructure of undoped MAO coating on TA2 pure titanium. No classic volcanic-pile deposits emerge on the coating surface, because $B_4O_7^{2-}$ introduced by $Na_2B_4O_7$ in the electrolyte increases the intensity of the spark discharge, dissolves the majority of the molten oxides, and generates a porous coating that differs from the usual crater. The majority of the molten oxides on the coating surface dissolve, resulting in a porous trabecular bone-like structure[27], which is 2 μm in width and has micrometer-sized pores, as shown in Fig.1e.

Fig. 1b – 1d show MAO coatings doped with nano-HA of different contents in the electrolyte. It can be seen that when the nano-HA content in MAO electrolyte increases, the number of connected grooves on the coated surface is gradually decreased, and the grooves evolve into independent pore structures. This phenomenon leads to a decrease in the coating porosity. It is reported that nano-HA particles exhibit excellent dispersibility in electrolyte solutions and typically possess negative surface charge characteristics[28–29]. Consequently, during MAO process, nano-HA is adsorbed to the anode and deposited into the micropores along with the spark discharges. As shown in Fig.1e–1h, with the addition of nano-HA, many prominent micro-particles begin to appear on the coating surface. When the nano-HA content in MAO

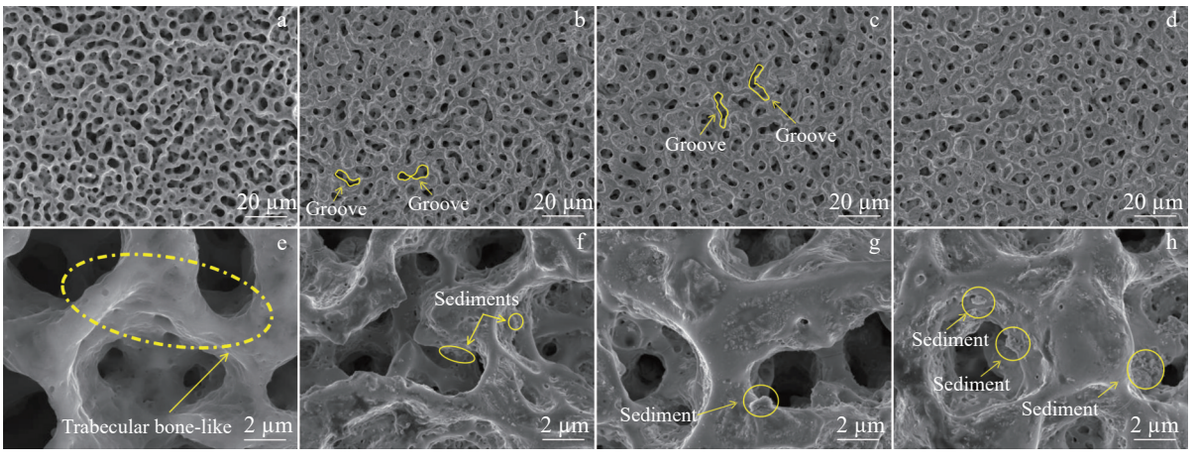

Fig.1 Low resolution (a–d) and high resolution (e–h) SEM images of undoped (a, e) and nano-HA-doped (b–d, f–h) MAO coatings prepared in electrolyte containing nano-HA of different contents: (b, f) 1 g/L HA; (c, g) 3 g/L HA; (d, h) 5 g/L HA

electrolyte is 3 g/L, obvious particle deposition can be observed. When the nano-HA content in MAO electrolyte further increases to 5 g/L, a large number of particles are deposited on the pore walls of the coating, and they are possibly identified as nano-HA particles.

Fig. 2 shows SEM image and corresponding EDS element mapping results as well as EDS spectrum of nano-HA-doped MAO coating prepared in electrolyte containing 3 g/L nano-HA. Significantly higher contents of elements Ca and P can be observed at the hole edges of the coating surface, whereas those at the pore interiors exhibit relatively lower values. It is suggested that the nano-HA particles may exist on the coating surface.

Fig. 3 shows content variations of elements Ca and P in nano-HA-doped MAO coatings prepared in electrolyte containing nano-HA of different contents. With the increase in nano-HA content in the electrolyte, the contents of elements Ca and P on the coating surface are also gradually increased. It is inferred that these deposits contain elements Ca and P.

Fig. 4 shows XRD patterns of the nano-HA-doped MAO coatings prepared in electrolyte containing nano-HA of different contents. The existence of HA diffraction peaks further proves that nano-HA-doped MAO coating contains nano-HA particles. Combining EDS results, the elements P and Ca observed in the micropores of MAO coating are another proof of the existence of nano-HA particles. According to Fig. 4, the coating is mainly composed of rutile phase, and anatase phase also exists. The rutile phase contains a greater number of hydroxyl (-OH) groups, compared with the anatase phase. The hydroxyl functional groups (Ti-OH and Si-OH) can effectively enhance the apatite-forming capacity by attracting the deposition of Ca^{2+} ions on the coating surface. Consequently, rutile phase with superior osteogenic performance enhances the biological activity through its enhanced apatite-forming capability[30]. When the arc discharge intensity during MAO is sufficiently high, the anatase phase in the coating is coarsened and irreversibly transformed into the rutile phase. After adding nano-HA particles into the electrolyte, when the voltage is reduced, there is a decrease in the transient temperature near the discharge channel of coating. This phenomenon leads to a higher content of residual anatase. Simultaneously, diffraction peaks of HA can be detected on the coating surface. Owing to the low deposition concentration, the intensity of HA peaks is relatively weak.

The detailed composition of nano-HA-doped MAO coating

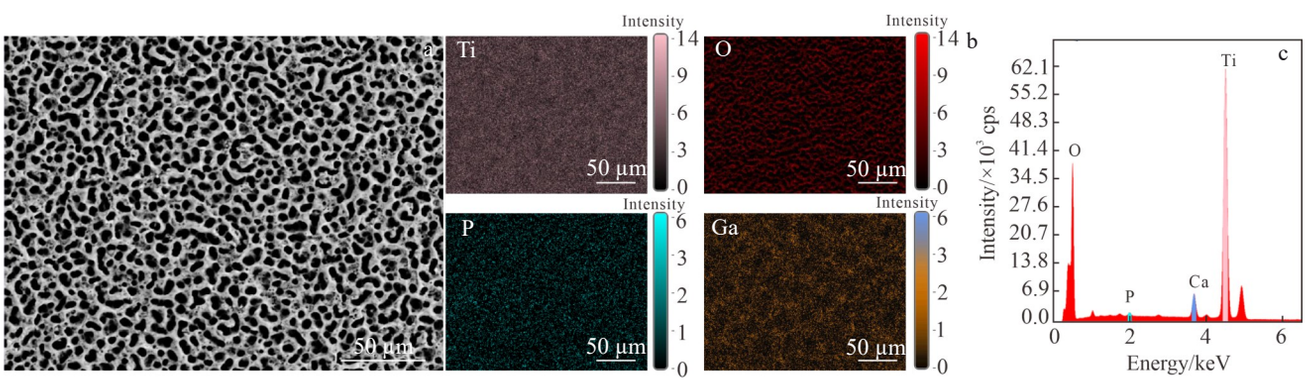

Fig.2 SEM image (a) and corresponding EDS element mapping results (b) as well as EDS spectrum (c) of nano-HA-doped MAO coating prepared in electrolyte containing 3 g/L nano-HA

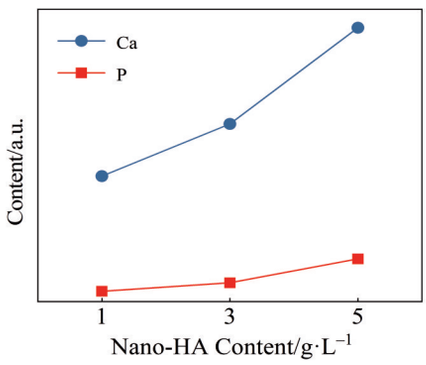

Fig.3 Content variations of elements Ca and P in nano-HA-doped MAO coatings prepared in electrolyte containing nano-HA of different contents

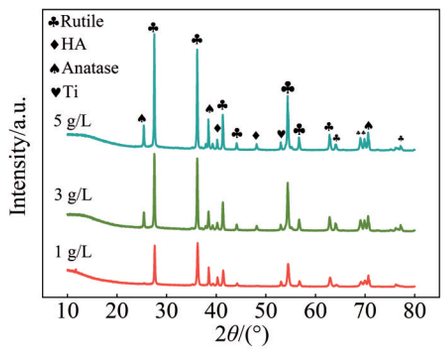

Fig.4 XRD patterns of nano-HA-doped MAO coatings prepared in electrolyte containing nano-HA of different contents

was analyzed by X-ray photoelectron spectroscopy (XPS). Fig. 5 shows XPS spectra of nano-HA-doped MAO coating prepared in electrolyte containing 3 g/L nano-HA. It can be seen that Ti 2p has two characteristic peaks at binding energies of 458.10 and 464.00 eV, which are related to TiO_2. According to Fig. 5c, two characteristic peaks at binding energies of 347.10 and 350.60 eV exist, corresponding to $Ca_3(PO_4)_2$. Fig. 5d shows a characteristic peak at the binding energy of 132.90 eV, which is related to the metallic phosphate. Therefore, it is suggested that HA is deposited on the coating surface in the form of $Ca_3(PO_4)_2$.

In summary, a micron-sized porous coating containing nano-HA particles was prepared on the surface of TA2 pure titanium by MAO technique, and the coating holes are uniformly distributed, showing the trabecular bone-like shape. Besides, the nano-HA is uniformly distributed around the discharge holes. With the increase in nano-HA content in the electrolyte, the number of nano-HA particles attached to the coating surface is also increased.

3.2 Microstructures of MAO coatings after HT treatment

The surface microstructure of biological implantation materials has a certain effect on the biological activity of implants[31]. Fig. 6 displays the surface morphologies of undoped and nano-HA-doped MAO coatings prepared in electrolyte containing 3 g/L nano-HA after HT treatment for different durations. Fig. 6a_3–6f_3 are magnified images of the areas marked by red circles in Fig.6a_2–6f_2, respectively. It can be seen that after HT treatment for different durations, nanostructures emerge on the coating surface. Without the addition of nano-HA particles, the cluster-like structures are mainly composed of nanosheets, as indicated by the yellow

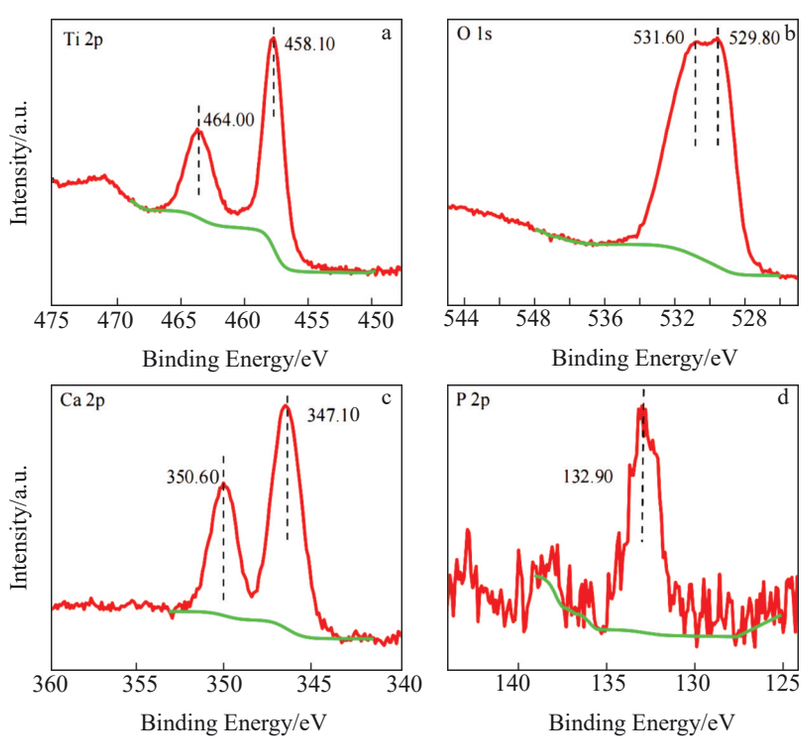

Fig.5 XPS spectra of nano-HA-doped MAO coating prepared in electrolyte containing 3 g/L nano-HA: (a) Ti 2p; (b) O 1s; (c) Ca 2p; (d) P 2p

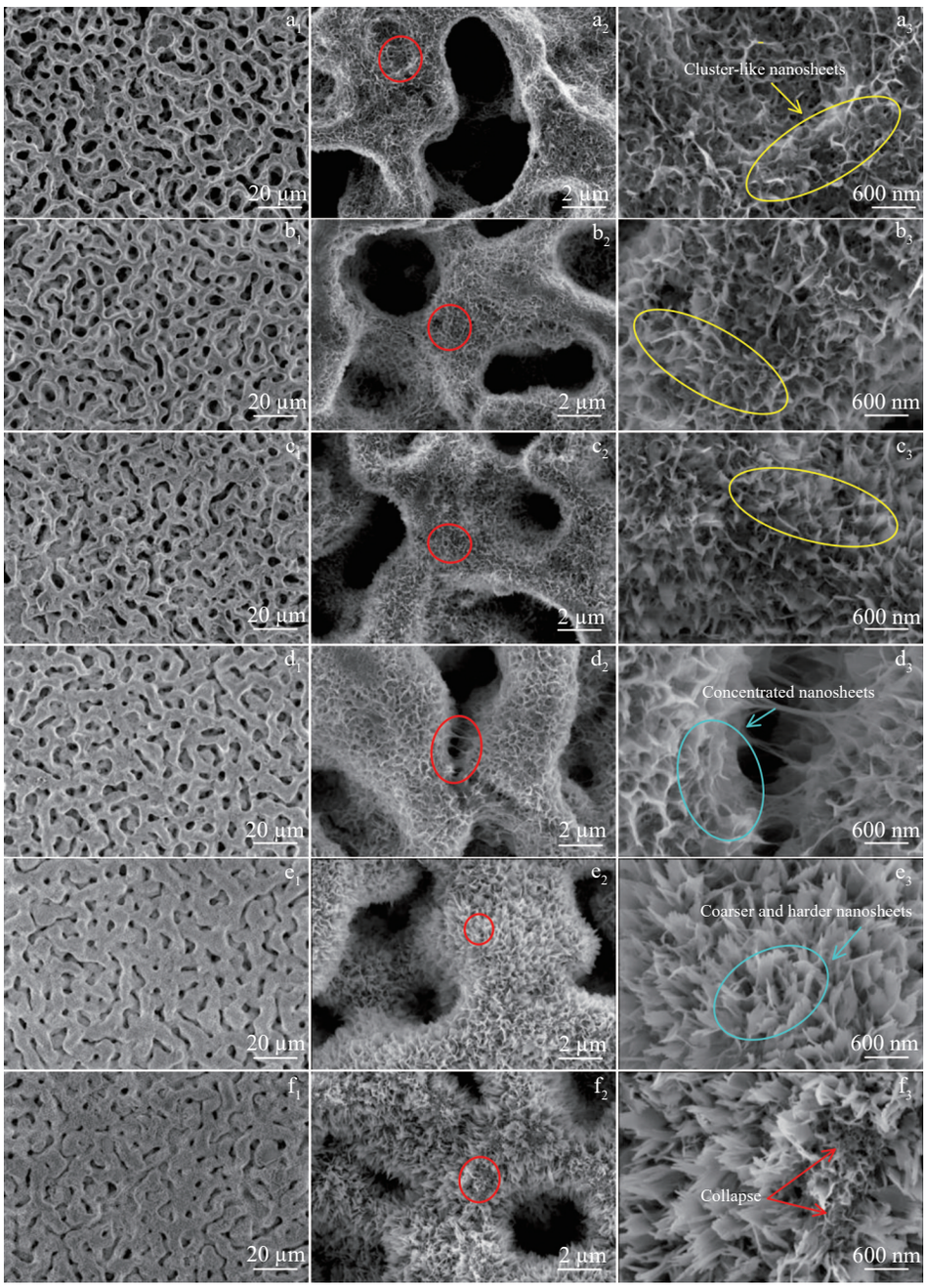

Fig.6 Surface morphologies of undoped (a_1–a_3, b_1–b_3, c_1–c_3) and nano-HA-doped (d_1–d_3, e_1–e_3, f_1–f_3) MAO coatings prepared in electrolyte containing 3 g/L nano-HA after HT treatment for 3 h (a_1–a_3, d_1–d_3), 6 h (b_1–b_3, e_1–e_3), and 12 h (c_1–c_3, f_1–f_3)

circles marked in Fig. $6a_3$–$6c_3$. The nanosheets are relatively thin, and the effect of HT treatment duration has a minimal impact on the nanosheets. As shown in Fig.$6d_3$, the nanosheets on the coating surface are concentrated. With the prolongation of HT treatment duration, these nanosheets on the coating surface are gradually transformed into coarser and harder phases, as indicated by the blue circles marked in Fig.$6d_3$–$6e_3$. However, as shown in Fig.$6f_3$, when HT treatment duration is prolonged to 12 h, the nanosheets start to collapse and easily fall off, significantly reducing the coating quality.

Fig.7 illustrates XRD patterns of the nano-HA-doped MAO coatings prepared in electrolyte containing 3 g/L nano-HA after HT treatment for 3, 6, and 12 h. It is evident that the phase composition of the MAO coating barely changes after HT treatment, and rutile and anatase phases are predominant. Additionally, the phase structure of coating surface exhibits minimal variation. This is because the film generated by HT treatment on MAO coating is relatively thin, and it does not change the phase structure.

3.3 Variations in porosity of micro/nano-structured coatings

The surface porosity of different coatings is depicted in Fig. 8. In Fig. 8, sample A is the undoped MAO coating; samples B–D are the nano-HA-doped MAO coatings prepared

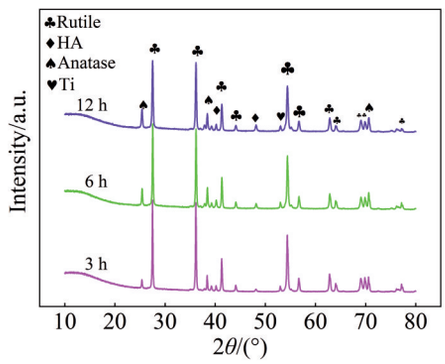

Fig.7 XRD patterns of nano-HA-doped MAO coatings prepared in electrolyte containing 3 g/L nano-HA after HT treatment for 3, 6, and 12 h

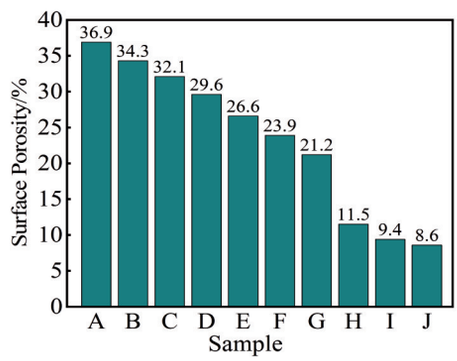

Fig.8 Surface porosity of different MAO coatings

in electrolyte containing 1, 3, and 5 g/L nano-HA, respectively; samples E – G are the undoped MAO coatings after HT treatment for 3, 6, and 12 h, respectively; samples H – J are the nano-HA-doped MAO coatings prepared in electrolyte containing 3 g/L nano-HA after HT treatment for 3, 6, and 12 h, respectively. It can be seen that the undoped MAO coating has the highest surface porosity of 36.9% among all the samples. This is because $B_4O_7^{2-}$ increases the intensity of spark discharge and dissolves most of the molten oxides, resulting in the formation of more surface pores on the coating with uniform distribution. When the electrolyte contains 1, 3, and 5 g/L nano-HA, the surface porosity of the resultant MAO coatings is 34.3%, 32.1%, and 29.6%, respectively. It is clear that the surface porosity of the coating shows a slight decrease after the addition of nano-HA particles. The larger the nano-HA content, the smaller the surface porosity. This is because during MAO process, nano-HA is adsorbed onto the anode and subsequently deposited into the micropores as a result of spark discharge. For the undoped MAO coatings after HT treatment, the surface porosity is 26.6%, 23.9%, and 21.2% when the HT treatment duration is 3, 6, and 12 h, respectively. It can be seen that the surface porosity of MAO coating significantly reduces after HT treatment. This is because the generated nanosheets are distributed on the MAO coating surface, exerting a hole-sealing effect on the coating surface. The surface porosity of the nano-HA-doped MAO coatings prepared in electrolyte containing 3 g/L nano-HA after HT treatment for 3, 6, and 12 h is 11.5%, 9.4%, and 8.6%, respectively. The surface porosity of these MAO coatings is lower than that of all other MAO coatings. It is speculated that during HT treatment, the doped HA preferentially forms a nanosheet structure, and it grows and adsorbs to the coating surface[32], therefore reducing the surface porosity.

3.4 Variations in roughness and hydrophilicity of micro/nano-structured coatings

The roughness of the coating surface is a crucial evaluation index for the biological activity of implants. A rougher surface can offer more anchoring points for cells and promote cell proliferation[33]. In serum, the proteins initially adsorbed onto the surface of titanium materials are predominantly albumin and fibronectin. The amount of these adsorbed proteins is positively correlated with the surface roughness of the titanium materials[34].

Appropriate implant surface roughness can promote earlier and stronger bone integration. A rough surface increases the contact area between the implant and bone tissue, therefore promoting the inward growth of bone tissue. Moreover, osteoblasts have better adhesion ability to rough surfaces. Fig. 9 shows 3D surface profiles (measured by AFM) of undoped MAO coatings before and after HT treatment for different durations. The surface roughness (R_a) value of undoped MAO coating before HT treatment is 21.8 nm, and that of undoped MAO coatings after HT treatment for 3, 6, and 12 h is 29.0, 30.3, and 40.0 nm, respectively. It can be inferred that the nanostructures are formed on the surfaces of all coatings after HT treatment, which improve the surface roughness of the coating. With the prolongation of HT treatment duration, the nanostructures on the coating continuously grow, therefore increasing the surface roughness.

Fig. 10 shows 3D surface profiles of nano-HA-doped MAO coatings prepared in electrolyte containing 3 g/L HA after HT treatment for 3, 6, and 12 h, whose R_a values are 46.9, 52.8, and 102.1 nm, respectively. With the prolongation of HT treatment duration, the nanostructures on the coating surface grow continuously, and the surface roughness is also increased. However, when the HT treatment duration is excessively long, the nanostructures may collapse or even fall off, which can lead to a decline in the coating performance. The surface roughness of all nano-HA-doped MAO coatings is higher than that of the undoped coatings. It is demonstrated that after HT treatment, the nano-HA-doped MAO coatings exhibit significantly coarser nanostructures on their surfaces.

Fig. 11 shows the water contact angles of different MAO coatings. In Fig. 11, samples A – C are the undoped MAO coatings after HT treatment for 3, 6, and 12 h, respectively; samples D–F are the nano-HA-doped MAO coatings prepared in electrolyte containing 3 g/L nano-HA after HT treatment for 3, 6, and 12 h, respectively. The hydrophilic properties of the material are closely related to its microscopic morphology of surface. It is reported that the surface wettability of the

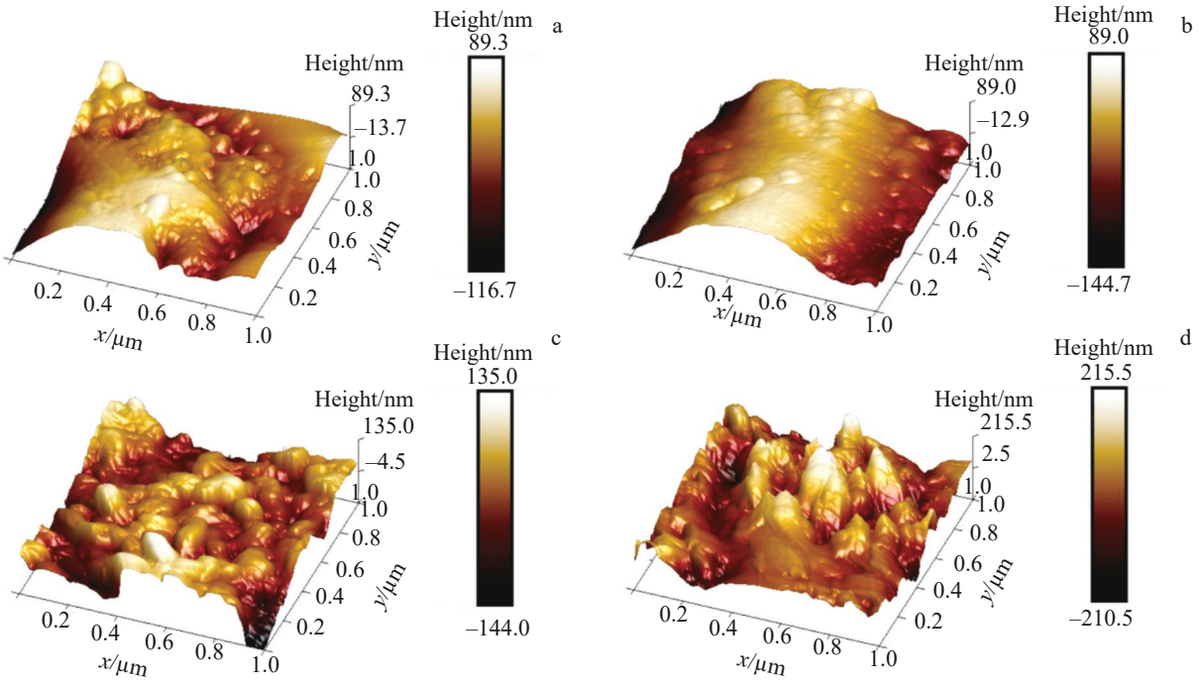

Fig.9 3D surface profiles of undoped MAO coatings before (a) and after HT treatment for 3 h (b), 6 h (c), and 12 h (d)

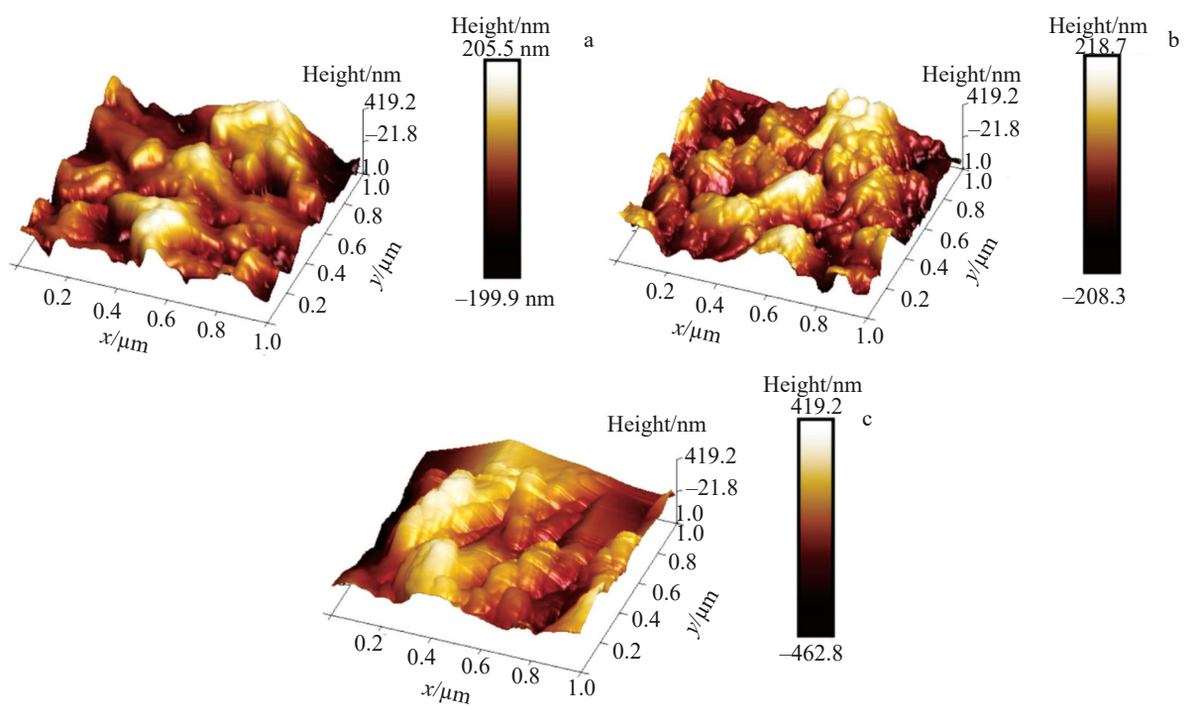

Fig.10 3D surface profiles of nano-HA-doped MAO coatings prepared in electrolyte containing 3 g/L HA after HT treatment for 3 h (a), 6 h (b), and 12 h (c)

implant has a significant impact on protein adsorption and osteoblast attachment. Besides, fibronectin and fibrinogen are more likely to adsorb on the hydrophilic surfaces, and the adsorbed proteins lead to an increase in the initial adhesion of osteoblasts[35–36]. The water contact angles of the undoped MAO coatings after HT treatment for 3, 6, and 12 h are 42.5°, 36.5° , and 20.3° , respectively. Notably, the water contact angles show a gradual reduction with the prolongation of HT treatment duration, revealing an inverse relationship with the surface roughness trend. It is known that the rougher the surface, the better the hydrophilicity. The water contact angles of the nano-HA-doped MAO coatings prepared in electrolyte containing 3 g/L nano-HA after HT treatment for 3, 6, and 12 h are 24.7°, 24.2°, and 14.0°, respectively. These nano-HA-doped MAO coatings exhibit higher surface roughness and superior hydrophilicity, compared with the abovementioned

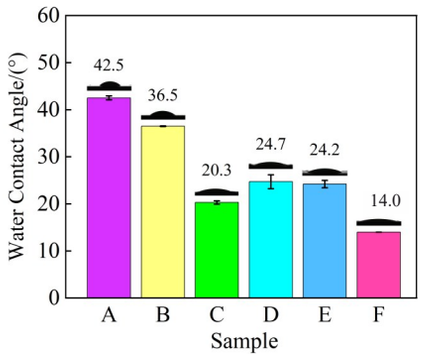

Fig.11 Water contact angles of different MAO coatings

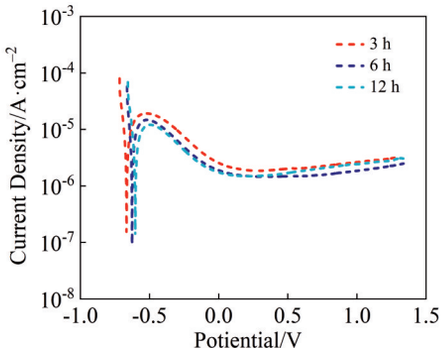

Fig.12 Polarization curves of nano-HA-doped MAO coatings prepared in electrolyte containing 3 g/L nano-HA after HT treatment for 3, 6, and 12 h

undoped MAO coatings. With the prolongation of HT treatment duration, the water contact angle is decreased. Hence, it is demonstrated that the coatings subjected to HT treatment have better hydrophilicity.

3.5 Corrosion resistance evolution of micro/nano-structured coatings in simulated body fluid

Fig. 12 illustrates the polarization curves of the nano-HA-doped MAO coatings prepared in electrolyte containing 3 g/L nano-HA after HT treatment for 3, 6, and 12 h. Table 3 presents the fitting results of polarization curves of nano-HA-doped MAO coatings prepared in electrolyte containing 3 g/L nano-HA after HT treatment for different durations. The corrosion potential (E_{corr}) and corrosion current density (I_{corr}) were analyzed using the Ec-lab software, and the polarization resistance (R_p) was subsequently calculated based on the Stern-Geary equation. The polarization resistance of the nano-HA-doped MAO coatings prepared in electrolyte containing 3 g/L nano-HA after HT treatment for 3, 6, and 12 h is 2.287×10^4, 2.467×10^4, and 2.290×10^4 Ω·cm^2, respectively. With the prolongation of HT treatment duration, the polarization resistance is initially increased and then decreased. This result indicates that the corrosion resistance of the coatings is firstly improved and then degraded.

The addition of nano-HA to the electrolyte can enhance the current density. The uniformly dispersed nano-HA particles enable more solutes to participate in MAO reaction and deposit on the coating surface, leading to the increase in coating roughness. The nano-HA particles deposited on the coating surface can enhance the corrosion resistance. To further confirm the impact of micro/nano-structure on the corrosion resistance of MAO coatings, electrochemical impedance spectroscopy (EIS) was used for analysis.

Table 3 Fitting results of polarization curves of nano-HA-doped MAO coatings prepared in electrolyte containing 3 g/L nano-HA after HT treatment for different durations

Duration/h	E_{corr}/V	$I_{corr}/\times10^{-5}$ A·cm^{-2}	Polarization resistance, $R_p/\times10^4$ Ω·cm^2
3	−0.6029	1.68	2.287
6	−0.6266	1.82	2.467
12	−0.6661	1.99	2.290

Fig.13 shows EIS results of nano-HA-doped MAO coatings prepared in electrolyte containing 3 g/L nano-HA after HT treatment for 3, 6, and 12 h. Gupta et al[37] found a direct relationship between electric arc radius and corrosion rate in the Nyquist diagram. With the prolongation of HT treatment duration from 3 h to 6 h, both the arc radius of the capacitive resistance and the impedance (denoted by $|Z|$) are increased. This result indicates an enhanced corrosion resistance of the coating. However, when the HT treatment duration is 12 h, the

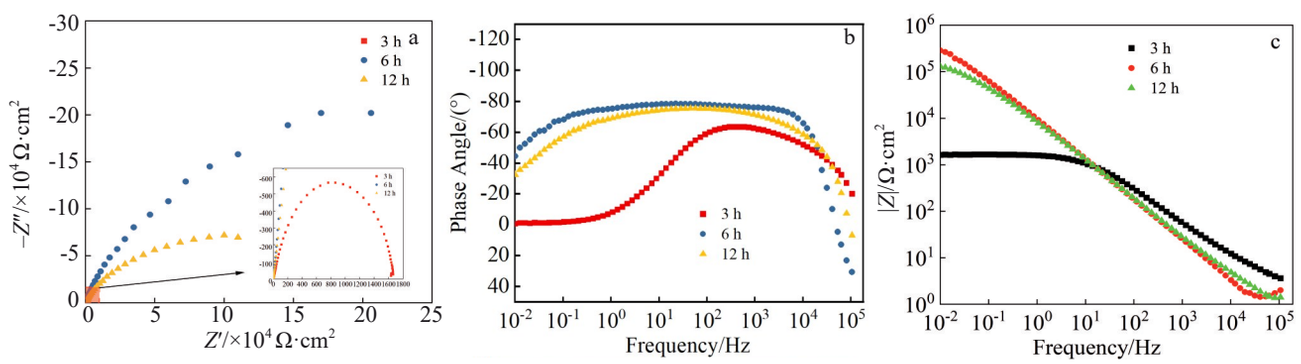

Fig.13 EIS results of nano-HA-doped MAO coatings prepared in electrolyte containing 3 g/L nano-HA after HT treatment for 3, 6, and 12 h: (a) $-Z''$ vs. Z'; (b) phase angle vs. frequency; (c) $|Z|$ vs. frequency

coating clusters become coarser and larger, and partial regions of the coatings even suffer collapse, leading to a substantial reduction in the corrosion resistance of the micro/nano-structured coating.

3.6 Cytocompatibility evaluation of micro/nano-structured coatings

The use of cell live-dead staining is a very intuitive method to determine the cell survival, and it is currently a common experimental method for detecting toxicity. Fig. 14 shows the fluorescent staining images of MC3T3-E1 cells cultured on different MAO coatings for 1, 3, and 5 d. It can be seen that after cell culture for 1 d, cells on coating surfaces show excellent spreading phenomenon. Some cells already present filopodia character and extend further into the surrounding regions. Compared with the MAO coatings before HT treatment, the micro/nano-structured surfaces of the MAO coatings after HT treatment provide more anchoring points for the cells, promoting the cell diffusion. HA can participate in bone mineralization, thus promoting bone integration of implants and natural bone[38]. It is demonstrated that elevated concentrations of calcium ions on the coating surface result in a substantial upregulation of $\alpha 5\beta 1$ integrin, which is closely associated with the matrix adhesion and cell activation. This integrin can mediate cell-substrate adhesion through binding with fibronectin. This process also generates intracellular signals that lead to an increase in cell proliferation[39–40]. Cell spreading is improved in the nano-HA-doped MAO coatings, compared with the undoped ones, and the number of cells is also increased after culture for 3 d. After HT treatment, the number of cells is greatly increased, compared with that on the MAO coating before HT treatment. After culture for 5 d, the cells spread over the entire surface of all MAO coatings. The bioactivity of the surface of all MAO coatings is markedly superior, particularly for the nano-HA-doped MAO coatings after HT treatment.

Fig. 15 shows MTT results of MC3T3-E1 cells cultured on the surface of different MAO coatings for 1, 3, and 5 d. In Fig. 15, sample A is the undoped MAO coating; sample B is nano-HA-doped MAO coating prepared in electrolyte containing 3 g/L nano-HA; sample C is undoped MAO coating after HT treatment; sample D is the nano-HA-doped MAO coating prepared in electrolyte containing 3 g/L nano-HA after HT treatment. The results show a significant upward trend in the number of cells on all coating surfaces with the prolongation of culture time, indicating that all MAO coating surfaces demonstrate excellent cytocompatibility. After culture for 1, 3, and 5 d, the nano-HA-doped MAO coating demonstrates significantly higher cell density, compared with the undoped MAO coating. In addition, the cell density becomes even higher on both MAO coatings after HT treatment. This phenomenon shows that the nano-HA-doped MAO coating exhibits higher biocompatibility in comparison with undoped MAO coating. Additionally, the cell proliferation ability can be further improved by HT treatment. This conclusion is in alignment with the results of cell live-dead staining analysis.

4 Analysis

The application of titanium and its alloys as biomedical implant materials still faces the following challenges in practical use: (1) insufficient bioactivity; (2) inadequate corrosion resistance. Therefore, the surface modification of titanium alloy biomaterials to obtain antibacterial property while enhancing cellular proliferation ability has become a key focus of current research. Introducing composite structures and bioactive elements to titanium implants is an

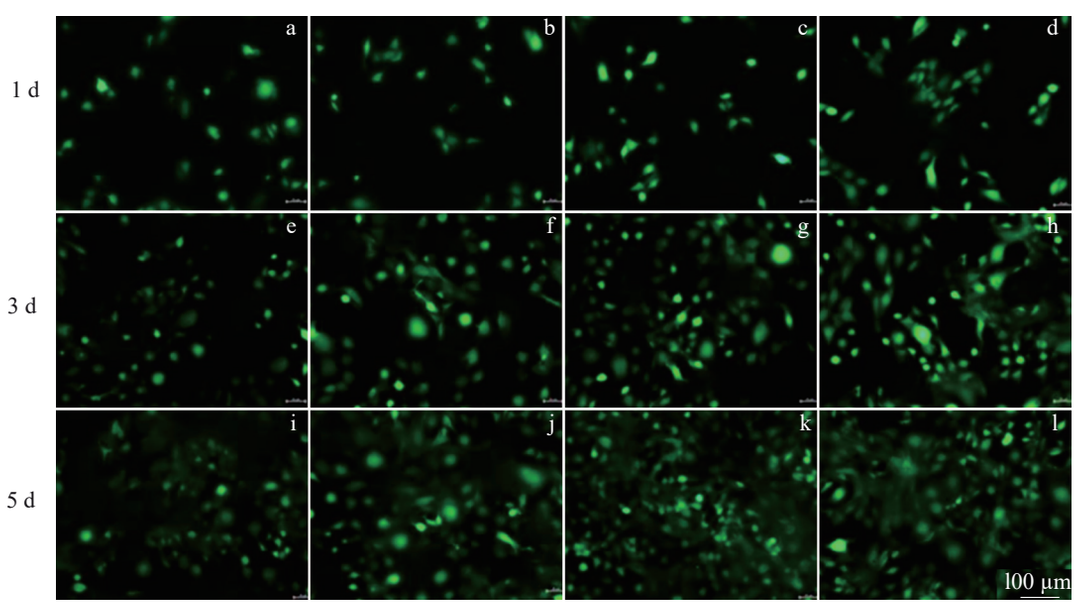

Fig.14 Fluorescent staining images of MC3T3-E1 cells cultured on different MAO coatings for 1 d (a–d), 3 d (e–h), and 5 d (i–l): (a, e, i) undoped MAO coating; (b, f, j) nano-HA-doped MAO coating prepared in electrolyte containing 3 g/L nano-HA; (c, g, k) undoped MAO coating after HT treatment; (d, h, l) nano-HA-doped MAO coating prepared in electrolyte containing 3 g/L nano-HA after HT treatment

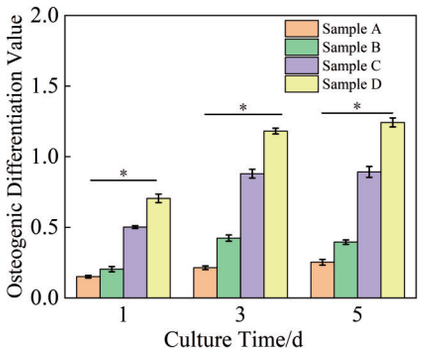

Fig.15 MTT results of MC3T3-E1 cell proliferation on different MAO coating surfaces (*: p<0.05)

effective method to improve osseointegration effect between bone and implants[41].

In Ref. [42 – 43], plasma spraying technique was used to prepare HA-containing composite coatings on titanium surfaces, demonstrating favorable biocompatibility. However, due to the high temperature and rapid cooling rate in the process, phase transformation may occur during spraying, and the bonding strength is insufficient. Therefore, it is necessary to select an appropriate powder mixture and specific heat treatment. Studies have shown that MAO coatings doped with metal ions have better bioactivity and antibacterial performance, and in-situ grown ceramic coatings demonstrate strong adhesion to the substrate. However, it is crucial to control and balance the doping content to ensure the biocompatibility and overall safety[44–46]. The HA doping process combined with the HT treatment can construct a micro/nano-structured MAO coating with high hydrophilicity, good biocompatibility, and high bonding strength on the surface of pure titanium.

As shown in Fig. 16, the micro/nano-structured composite coating can be prepared by HT treatment of undoped and nano-HA-doped MAO coatings. After nano-HA doping and HT treatment, numerous densely-aggregated nanosheet-like structures emerge on the coating surface. With the prolongation of HT treatment duration, the nanosheets are concentrated on the surface, and this change is more pronounced on the nano-HA-doped MAO coating. When the HT treatment duration is 6 h, the nanostructures of the coating are transformed from nanosheet-like to nanocluster-like morphology, accompanied by the increase in surface roughness. However, when the HT treatment duration is prolonged to 12 h, the nano-lamellar structure begins to collapse and exhibits easy detachment, indicating a significant deterioration in coating quality. It is evident that the introduction of nano-HA can facilitate the formation of micro/nano-structures. Moreover, under appropriate HT temperature and duration conditions, it can further refine the micro/nano-structures of the coating surface.

Jin et al[47] prepared superhydrophilic $Mg(OH)_2$ films on AZ31B magnesium alloy substrate through HT treatment. They proposed that the flake $Mg(OH)_2$ surface was enriched with abundant hydroxyl groups (-OH), which endowed the film with superhydrophilic properties. With the prolongation of HT treatment duration, the aggregation of nanosheets in the HA-doped MAO coating significantly improves the surface roughness. Consequently, the surface roughness of the HT-treated HA-doped MAO coating rises from 21.8 nm (the surface roughness of the untreated MAO coating) to 102.1 nm, representing an approximately fivefold increase. This result also leads to a reduction in the water contact angle of the coating from 42.5° to 14.0°, which is likely due to the increased water-holding capacity of the rough and porous surfaces. Hydrophilicity is critical for the biocompatibility of bone-tissue implants, as it influences cell attachment and growth[48]. As shown in Fig. 11, the excellent hydrophilicity of the nano-HA-doped MAO coatings after HT treatment can be attributed to the presence of -OH groups, which can be identified through XPS analysis results (Fig. 5). HT treatment forms a large number of nanoflake structures on the MAO coatings, increasing the contact area at the solid-liquid interface and enhancing the hydrophilic properties. Additionally, the larger surface roughness of the coating will further promote the hydrophilic performance due to capillary adsorption[49]. These results suggest that the construction of micro/nano-structures may serve as an effective method to promote cell adhesion and growth.

Cytotoxicity assays and MC3T3-E1 cell proliferation tests demonstrate that the nano-HA-doped MAO coatings after HT treatment on titanium surfaces exhibit no cytotoxicity.

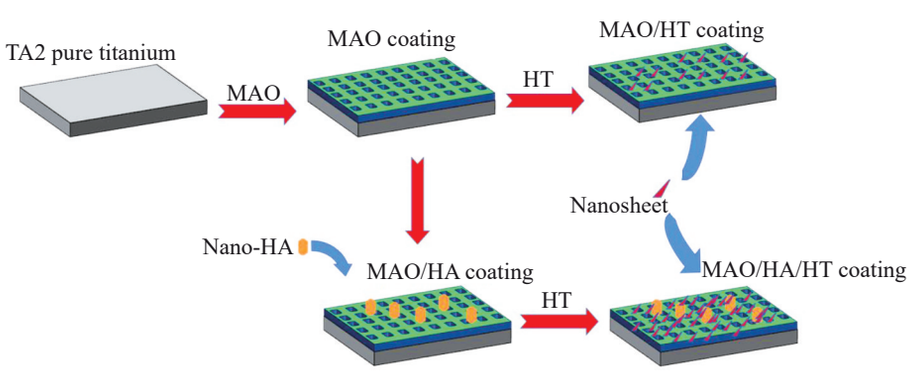

Fig.16 Preparation mechanism of micro/nano-structured composite coatings

Furthermore, the cellular bioactivity is significantly enhanced with the addition of nano-HA. Significant enhancement in both cell population density and number can be observed for all the nano-HA-doped or HT-treated MAO coatings, compared with the undoped MAO coating. Notably, HT-treated coatings exhibit higher cell numbers and density by more than two orders of magnitude, compared with their non-HT-treated counterparts. Thus, the optimal biocompatibility is achieved for the nano-HA-doped MAO after HT treatment (micro/nano-structured composite coating). This phenomenon may be attributed to the characteristics of the micro/nano-structures: the channels formed by the micro/nano-structures are more suitable for the adhesion and growth of cells[50]. Simultaneously, the micro/nano-structured coatings containing nano-HA demonstrate stronger biocompatibility, compared with the ones without nano-HA doping. This is because HA has good bioactivity, which can participate in the in-vivo metabolic process, facilitate the repair of damaged tissues, and promote the protein adsorption on the coating surface. Besides, the incorporation of nano-HA can increase the surface area of the coating, providing more space for cell growth and further facilitating cellular adhesion and permeation. More importantly, the nano-HA doped into the MAO coating promotes the growth of nanosheets generated by HT, but the precise growth mechanism remains unclear.

Shi et al[51] studied the synergistic effect of micro/nano-structures and Cu^{2+}-doped HA particles on the osteoblast viability and antibacterial activity. They fabricated Cu^{2+}-doped HA with micro/nano-structures via HT method. That micro/nano-structure exerts better hydrophilicity and concurrently promotes the adhesion, proliferation, and osteogenic differentiation of RCOs. The research indicates that the micro/nano-structure facilitates protein interaction and may promote osteoblast adhesion. Furthermore, the HA-containing micro/nano-structured ceramic coating enhances the cell activity through the activation of integrin signaling pathways, such as extracellular signal-regulated kinases. Xu et al[52] prepared TiO_2-HA coating on ultrafine pure titanium by combining MAO and HT treatment. The results show that the synergistic effect of the micro/nano-structures and HA plays an effective role in the adhesion, proliferation, and differentiation of osteoblasts.

Hence, it can be inferred that the synergistic effect of the micro/nano-structures (microscale pores with nanosheets) and nano-HA doping can improve the cellular proliferation on the coating surface. Consequently, excellent biocompatibility for cellular activities can be achieved on the titanium alloy surface.

5 Conclusions

1) The undoped MAO coating presents a trabecular bone-like porous structure. After incorporating nano-HA into the electrolyte, nano-HA is deposited around the discharge channels, and the doped coating is predominantly composed of rutile TiO_2. HA can be formed on the coatings, and the larger the HA doping content, the more the nano-HA formed on MAO coating.

2) HT treatment facilitates the formation of nanoflake structures on the coating surface. With the prolongation of HT treatment duration, the clusters of the coating are gradually coarsened. However, excessively prolonged HT treatment duration may lead to collapse or fall off of the coating. The micro/nano-structured nano-HA-doped MAO coating after HT treatment exhibits larger particle size, increased surface roughness, and enhanced hydrophilicity. The film generated by HT treatment remains relatively thin and cannot change the phase composition of the coating.

3) The micro/nano-structured coatings fabricated on the TA2 pure titanium surface exhibit excellent cell spreading effect and proliferation performance without cytotoxicity. In addition, the synergistic effect of nano-HA and micro/nano-structures on the coating surface greatly promotes the cell proliferation, presenting non-cytotoxic characteristic, and indicating that the coating possesses good biocompatibility.

4) The coating performance achieves optimal state when the MAO coating is prepared with 3 g/L HA and HT-treated for 6 h. In this case, the water contact angle is as low as 24.2°, and the polarization resistance is as high as $2.467\times10^4\ \Omega\cdot cm^2$.

References

1 Chen X D, He S H, Dong Y L *et al. Materials Today Bio*[J], 2024, 24: 100912

2 Li X, Zhao Y C, Yin D F *et al. Advanced Healthcare Materials* [J], 2025, 14(6): e2403626

3 Gerhátová Ž, Paták J, Babincová P *et al. Journal of Physics: Conference Series*[J], 2024, 2712: 012006

4 Xu Jianbo, Zhang Bowen, Qu Wentao *et al. Rare Metal Materials and Engineering*[J], 2024, 53(5): 1296 (in Chinese)

5 Elliott D T, Wiggins R J, Dua R. *Journal of Biomedical Materials Research Part B: Applied Biomaterials*[J], 2021, 109(7): 973

6 Liu Z Y, Zhao M C, Yin D F *et al. Acta Biomaterialia*[J], 2025, 192: 1

7 Ali S H, Thair L, Hanaa D A *et al. Journal of Bio- and Tribo-Corrosion*[J], 2019, 5(4): 85

8 Gupta M, Markocsan N, Li X H *et al. Journal of Thermal Spray Technology*[J], 2018, 27(1): 84

9 Li X W, Zhang J H, Feng Y X *et al. Rare Metal Materials and Engineering*[J], 2024, 53(10): 2777

10 Gao Fuhao, Lv Binjiang, Guo Feng *et al. Rare Metal Materials and Engineering*[J], 2025, 54(1): 171 (in Chinese)

11 Feng J, Yuan S H, Shi Z Y *et al. Journal of Materials Research and Technology*[J], 2025, 36: 6486

12 Feng J, Li B W, Chen W B *et al. Rare Metal Materials and Engineering*[J], 2021, 50(11): 3896

13 Gao J P, Lv Y J, Li Y J *et al. Rare Metal Materials and Engineering*[J], 2025, 54(5): 1127

14 Feng Jun, Li Biwen, Chen Wenbo *et al. Rare Metal Materials and Engineering*[J], 2020, 49(7): 2229 (in Chinese)

15 Zhang Z Y, Huang T Y, Zhai D J *et al. Surface and Coatings Technology*[J], 2022, 451: 129045

16 Selvi E, Muhaffel F, Yürektürk Y *et al. Journal of Materials*

Engineering and Performance[J], 2022, 31(2): 1667
17 Zhu J C, Li H Z, Li Z X *et al. Coatings*[J], 2022, 12(10): 1538
18 Manivasagam V K, Popat K C. *Materials Science and Engineering C: Materials for Biological Applications*[J], 2021, 128: 112315
19 Wang W Z, Li X, Zhao C C *et al. Composites Part B: Engineering*[J], 2025, 298: 112379
20 Wang B Y, Zhang K K, Fan Y C *et al. Rare Metal Materials and Engineering*[J], 2025, 54(4): 854
21 Xie M Y, Zhong Y C, Wang S Q *et al. Materials Chemistry and Physics*[J], 2022, 292: 126872
22 Webster T J, Ergun C, Doremus R H *et al. Journal of Biomedical Materials Research Part A*[J], 2000, 51(3): 475
23 Banerjee D, Majumdar U, Bose S. *Journal of Materials Research*[J], 2024, 39(20): 2843
24 Li C, Yang Y, Yang L J *et al*. *Molecules*[J], 2020, 25(7): 1494
25 Xu Yiku, Luo Yuqing, Jiang Jianli *et al. Rare Metal Materials and Engineering*[J], 2023, 52(2): 675 (in Chinese)
26 Li B B, Yang T, Sun R X *et al. Dental Materials Journal*[J], 2021, 40(2): 455
27 Wang Weiqiang, Wang Shuyue, Yu Fengyun *et al. Surface Technology*[J], 2023, 52(4): 363 (in Chinese)
28 Irfan M, Suprajaa P S, Praveen R *et al. Materials Letters*[J], 2021, 282: 128685
29 Meng L Z, Shu M M, Mei P *et al. BMC Oral Health*[J], 2025, 25(1): 204
30 Zhao J H, Liu L, Ma F C *et al. Ceramics International*[J], 2025, 51(10): 13090
31 Zhang Y Y, Fan Z M, Xing Y H *et al. Frontiers in Bioengineering and Biotechnology*[J], 2022, 10: 981062
32 Yigit O, Dikici B, Ozdemir N. *Journal of Materials Science: Materials in Medicine*[J], 2021, 32(4): 40
33 Ding R K, Nathaniel C M, Woeppel K M *et al. Langmuir*[J], 2022, 38(24): 7512
34 Barberi J, Spriano S. *Materials*[J], 2021, 14(7): 1590
35 Arun M, Joselin R, Abdul A M I *et al. Innovative Infrastructure Solutions*[J], 2023, 8(5): 155
36 Song Z Z, Cai Y, Li X *et al. Materials Horizons*[J], 2025, 12(3): 814
37 Gupta A, Hiremath S S. *Surface and Coatings Technology*[J], 2024, 477: 130288
38 Asimeng B O, Agyen E O, Asiamah R *et al. Journal of the Australian Ceramic Society*[J], 2022, 58(4): 1321
39 Liang L X, Lin Z J, Duan Z Q *et al. Regenerative Biomaterials*[J], 2024, 11: rbae104
40 Wu M Y, Zhao M C, Cai Y *et al. International Journal of Extreme Manufacturing*[J], 2024, 6(6): 062010
41 López-Valverde N, Flores-Fraile J, Ramírez J M *et al. Journal of Clinical Medicine*[J], 2020, 9(7): 2047
42 Pillai R S, Frasnelli M, Sglavo V M. *Ceramics International*[J], 2018, 44(2): 1328
43 Kowalski S, Gonciarz W, Belka R *et al. Coatings*[J], 2022, 12(9): 1317
44 Wang X J, Mei L N, Jiang X S *et al. Frontiers in Bioengineering and Biotechnology*[J], 2021, 9: 625877
45 Kobayashi M, Shimabukuro M, Aoki S *et al. Materials Letters*[J], 2024, 377: 137531
46 Liu Y C, Xu T W, Sun B Q *et al. Journal of Materials Research*[J], 2022, 37(16): 2675
47 Jin Q, Tian G Y, Li J X *et al. Colloids and Surfaces A: Physicochemical and Engineering Aspects*[J], 2019, 577: 8
48 Chen S C, Guo Y L, Liu R H *et al. Colloids and Surfaces B: Biointerfaces*[J], 2018, 164: 58
49 Bamorovat A G, Bahrami M. *Scientific Reports*[J], 2022, 12(1): 14867
50 Yuan Z, Liu P, Liang Y N *et al. Journal of Materials Chemistry B*[J], 2018, 6(9): 1359
51 Shi F, Liu Y M, Zhi W *et al. Biomedical Materials*[J], 2017, 12(3): 035006
52 Xu L, Li J Q, Xu X J *et al. ACS Applied Materials & Interfaces*[J], 2019, 11(51): 47680

用于纯钛的纳米羟基磷灰石掺杂微/纳结构复合微弧氧化涂层的制备与性能

冯　军，邓胜勇，赵颖超，成俊杰，杨旭东
(南华大学 机械工程学院，湖南 衡阳 421001)

摘　要：通过微弧氧化（MAO）-水热（HT）技术在TA2纯钛表面制备了一种由二氧化钛（TiO_2）和羟基磷灰石（HA）组成的微/纳米结构复合涂层，以提高钛的耐腐蚀性能和生物相容性。通过扫描电子显微镜探究了涂层的表面微观形貌；通过原子力显微镜、水接触角探究了涂层的粗糙度和亲水性；在模拟人体体液中通过电化学阻抗谱和动电位极化测试评估了涂层的耐腐蚀性能；通过体外细胞培养实验研究了生物相容性。结果表明，通过在MAO电解液中掺杂纳米HA，可以获得负载纳米HA颗粒的微米级涂层，再进行HT处理，可以获得具有纳米片状结构的含HA微/纳米结构复合涂层。该微/纳结构复合涂层具备良好的亲水性和耐腐蚀性能。当在MAO电解液中掺杂3 g/L HA并HT处理6 h时制得的涂层性能最佳，水接触角为24.2°，极化电阻最大为2.467×10^4 Ω·cm^2。此外，涂层表面的纳米HA和微/纳结构的协同作用极大地促进了细胞增殖，展现出无细胞毒性，说明涂层具备良好的生物相容性。

关键词：微弧氧化；水热法；纳米HA；微/纳结构

作者简介：冯 军，男，1979年生，博士，副教授，南华大学机械工程学院，湖南 衡阳 421001，E-mail: speedfjkang@163.com